Letter

Determining ground states of alloys by a symmetry-based classification

Yu-Jie Cen,* Chang-Chun He,* Shao-Bin Qiu, Yu-Jun Zhao, and Xiao-Bao Yang†
School of Physics and Optoelectronics, South China University of Technology, Guangzhou 510640, People's Republic of China

(Received 11 January 2022; revised 4 April 2022; accepted 20 April 2022; published 17 May 2022)

Reducing the number of candidate structures is crucial to improve the efficiency of global optimization. Herein, we demonstrate that the generalized Hamiltonian can be described by the atom classification model (ACM) based on symmetry, generating competent candidates for the first-principles calculations to determine ground states of alloy directly. The candidates can be obtained in advance through solving the convex hull step by step because the correlation functions of the ACM can be divided into various subspace according to the defined index l. As an important inference, this index can be converted to the number of Wyckoff positions, revealing the dominant effect of geometry symmetry on structural stability. Taking Ni-Pt, Ag-Pd, Os-Ru, Ir-Ru, and Mo-Ru as examples, we not only identify the stable structures in previous theoretical and experimental results, but also predict a dozen of configurations with lower formation energies, such as $Ag_{0.5}Pd_{0.5}$ (Fd-$3m$), $Os_{0.5}Ru_{0.5}$ ($Pnma$), $Ir_{1/3}Ru_{2/3}$ ($P6_3/mmc$), and $Mo_{0.25}Ru_{0.75}$ ($Cmcm$).

DOI: 10.1103/PhysRevMaterials.6.L050801

Determining the material structure theoretically will provide important guidance to the experiment where the energy evaluation and structure evolution are two main steps to predict the ground-state (gs) structure. To explore configuration space, *ab initio* random structure searching [1], USPEX [2], and CALYPSO [3] have been successively developed based on the global optimization, which are widely used in the discovery of materials [4–7].

For the alloy systems, the cluster expansion (CE) method uses the linear combination of basis functions to describe the Hamiltonian [8] and fits the interaction parameters through the data from density functional theory. To balance efficiency and accuracy, the effective cluster interactions should be selected for each specific material. Based on the genetic algorithm, a few of the interaction parameters can be selected from a large number of interaction parameters, which can produce a good fitting of the Hamiltonian in some systems [9]. In addition, the parameters of the CE can be selected by using prior probability distribution combined with simple models or experience, based on the framework of Bayes' theorem [10].

Besides the simplification of energy evaluations, reducing the number of candidate structures is practical to accelerate global optimization. Instead of scanning the interaction parameter space [11], the possible ground-state structures of the system can be determined by finding convex hull in the feasible domain of the correlation function space by establishing geometric inequality constraints [12–15]. By enumerating the structures of unique supercells of finite volume, the convex hull of the feasible region in the CE correlation function space can be directly solved to obtain the possible ground-state structures of binary alloy [16]. Based on simple geometric characteristics, the amount of the average bond type is used to evaluate the degree of deviation of the structure from a random situation, and the candidates with a larger average bond type will be ground-state structures [17]. It is comprehensible that these structures are closer to the edge of the feasible region in the correlation function space, approaching the convex hull.

Most previous studies focused on the acceleration of energy evaluations with high accuracy combining the first-principles calculations and the interaction potential model [18–21]. It is worth noting that the ground states of the alloy are dominated by the energy model in which the selection of parameters is closely related to the cutoff radii (R_{cut}) and the training data set [22]. To screen candidates before energy evaluations, it will become difficult to solve the convex hull in the CE when the dimensionality of the correlation function space increases with the increasing of interactions. For a set of n points in $\mathbb{R}^d$, the regular triangulations algorithm takes $O(n \log n + n^{d/2})$ time [23,24], making it impossible to achieve medium-sized inputs when the function space exceeds ten dimensions.

In this Letter, we show that the ground-state structures of alloys can be directly obtained by the first-principles calculations where the candidates are screened by the symmetry-based classification. First, we demonstrate that the atom classification model (ACM) in our previous study [25] is equivalent to CE considering the complete many-body interaction, and the classified atoms correspond to Wyckoff positions for the infinite R_{cut}. Second, we propose an effective method for calculating the convex hull with a given R_{cut}, and the convex hull can be solved step by step in a certain order by dividing the correlation functions of the ACM into various subspace. Finally, we provide a high-throughput first-principles calculations strategy to explore the stable structures of alloys, reducing the number of candidates significantly.

As shown in Fig. 1(a), there are 272 8670 unique configurations of A_xB_{1-x} within 20 atoms in the fcc lattice. With the truncation of the tetrahedron, there are five possible ground-state structures according to the convex hull of the ACM. These structures are the typical ordered phase ($L1_0$

*These authors contributed equally to this work.
†scxbyang@scut.edu.cn

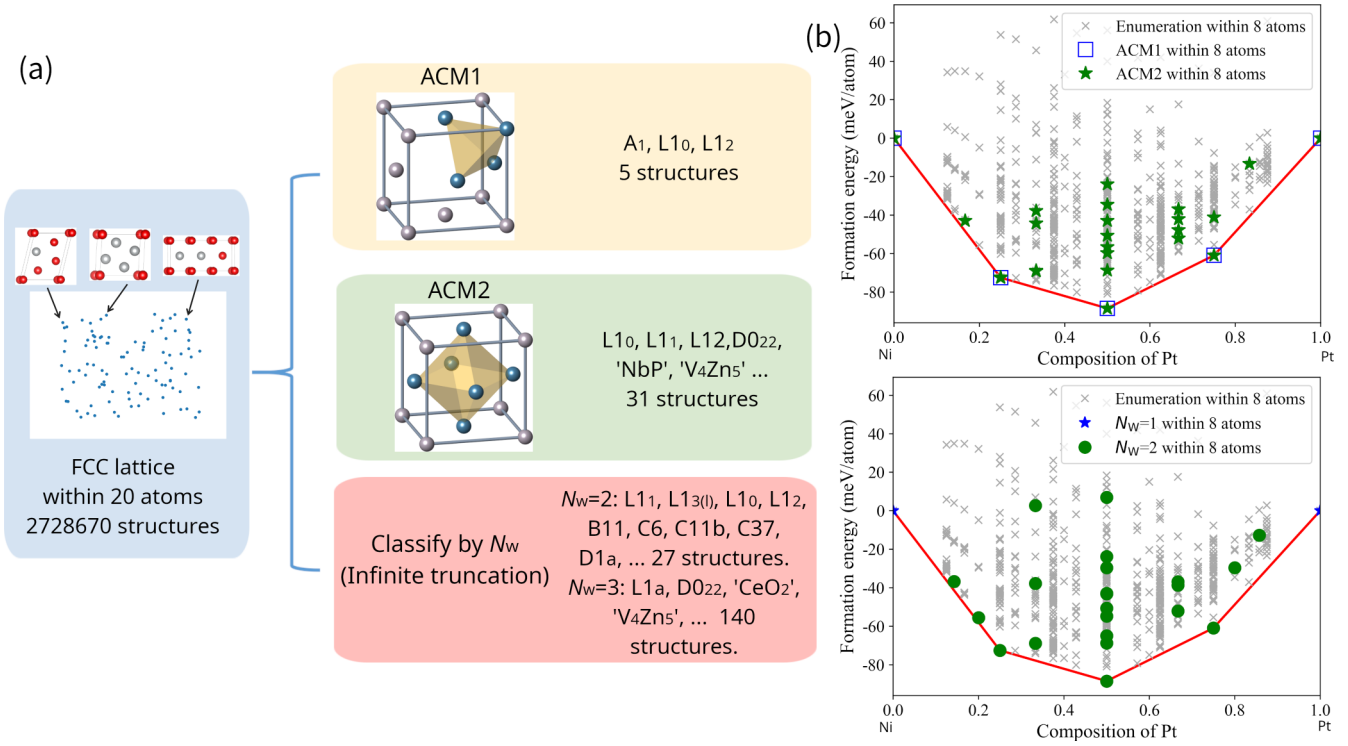

FIG. 1. (a) The fcc-derivative structures within 20 atoms are filtered by the ACM with various R_{cut} and the number of Wyckoff positions, and the order phases are obtained. (b) The formation energy of Ni-Pt alloy with cells within eight atoms.

and $L1_2$) found in various binary alloys, such as Cu_xAu_{1-x} and Ni_xPt_{1-x}. The number of vertex structures will increase to 31, and more ground-state structures in experiment are conformed when the truncation is expanded to the octahedron. Meanwhile, most ordered alloy structures in the fcc lattice can be obtained by considering the candidates with the number of Wyckoff positions (N_{W}) no more than three. In the case of Ni_xPt_{1-x} [shown in Fig. 1(b)], all the five ground-state structures can be determined after the calculations of candidates obtained by the ACM with the truncation of the tetrahedron. The first-principles calculations [26–28], details are shown in Supplemental Material (SM) [29], Sec. 1. For a larger truncation of the octahedron, no new stable structures are found. Similarly, the five ground-state structures can be reproduced in 29 candidates with $N_{\text{W}} \leqslant 2$, and no new stable structures are uncovered in the 140 candidates with $N_{\text{W}} = 3$.

Generally, the ground-state structures of the material are highly symmetric in geometry. In the following, we show N_{W} is the key index to describe the structural stability and the symmetry, through a concise demonstration based on the ACM. Taking the one-dimensional atomic chain as an example [as shown in Fig. 2(a)], we construct the linear Hamiltonian based on the original lattice-gas model (LGM) [30], the CE, and the ACM as follows:

$$H = \boldsymbol{J} \cdot \overline{\boldsymbol{\Pi}}, \tag{1}$$

where $\boldsymbol{J}$ is the interaction parameter and $\overline{\boldsymbol{\Pi}}$ is the correlation function shown in Table I. The deduction of the ACM is in SM, Sec. 2.1 [29].

In the representation of the CE and ACM [see Figs. 2(b) and 2(c)], we have determined the possible ground-state structures of the system by finding the vertices in the feasible region of the correlation function space by enumerating all the structures of the one-dimensional atomic chain of binary alloys within eight atoms. With the transformation matrix [see Fig. 2(b)], the correlation functions of the ACM and CE can be converted to each other, confirming the equivalence of these two methods in energy evaluation in the framework of the LGM. In addition, we have demonstrated that the ACM is

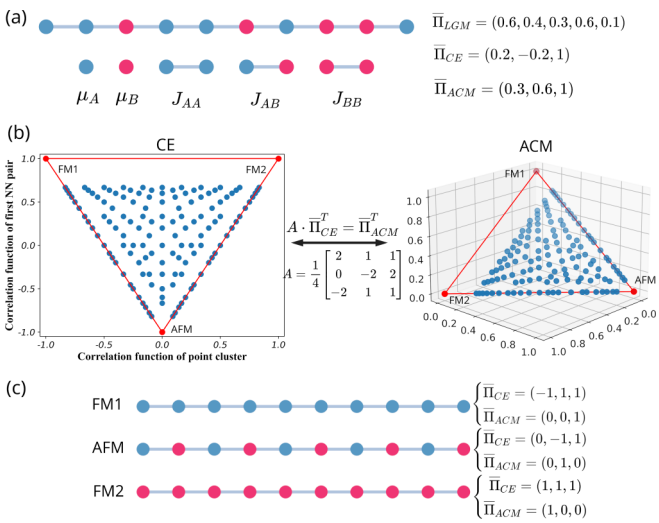

FIG. 2. (a) On the left side is a random periodic one-dimensional (1D) atomic chain and five interaction types. On the right side is the correlation functions in the LGM, the CE, and the ACM. (b) The correlation functions space of the CE and the ACM. (c) Three convex hull structures and their corresponding correlation functions.

TABLE I. The components of J and $\overline{\Pi}$ in the LGM, the CE, and the ACM.

	J	$\overline{\Pi}$
LGM	$J_1 = \mu_A$, $J_2 = \mu_B$, $J_3 = J_{AA}$, $J_4 = J_{AB}$, $J_5 = J_{BB}$	$\Pi_1 = \frac{1}{N}\sum_i P_i^A$, $\Pi_2 = \frac{1}{N}\sum_i P_i^B$, $\Pi_3 = \frac{1}{N}\sum_{i,j} P_i^A P_j^A$, $\Pi_4 = \frac{1}{N}\sum_{i,j}(P_i^A P_j^B + P_i^B P_j^A)$, $\Pi_5 = \frac{1}{N}\sum_{i,j} P_i^B P_j^B$
CE	$J_1 = \frac{1}{2}(J_{AA} - J_{BB} + \mu_A - \mu_B)$, $J_2 = \frac{1}{4}(J_{AA} - 2J_{AB} + J_{BB})$, $J_3 = \frac{1}{4}(J_{AA} + 2J_{AB} + J_{BB} + 2\mu_A + 2\mu_B)$	$\Pi_1 = \frac{1}{N}\sum_i S_i$, $\Pi_2 = \frac{1}{N}\sum_{i,j} S_i S_j$, $\Pi_3 = 1$
ACM	$J_1 = \mu_A + J_{AA}$, $J_2 = \frac{1}{2}(\mu_A + \mu_B + J_{AB})$, $J_3 = \mu_B + J_{BB}$	$\Pi_1 = \frac{1}{4N}\sum_{i,j}(1 + 2S_i + S_i S_j)$, $\Pi_2 = \frac{1}{4N}\sum_{i,j}(2 - 2S_i S_j)$, $\Pi_3 = \frac{1}{4N}\sum_{i,j}(1 - 2S_i + S_i S_j)$

equivalent to the CE when the complete many-body interactions are considered. For the two-dimensional square lattice truncating to next-neighbor interaction, there are 20 kinds of interactions in the LGM, and the system can be equivalently represented by six kinds of four-body interactions in the ACM, where all the two- and three-body interactions are included according to the deduction (see the SM, Sec. 2.2 [29]).

Although more parameters are required in the ACM compared with the CE, the correspondence between the cluster environment in the ACM, and the structure is clearer, revealing the relation of structural stability and the symmetry of configuration. More importantly, with the benefit of the non-negative components of correlation functions, the ACM brings convenience for the subsequent calculation of convex hulls to find possible ground-state structures.

Mathematically, the vertices of a set is defined as follows: in a point set $X = \{\boldsymbol{x}_1, \boldsymbol{x}_2, \boldsymbol{x}_3,...\}$ with any point $\boldsymbol{x}_i$ belonging to X, the convex set is marked as $Y = \{\boldsymbol{y}_1, \boldsymbol{y}_2, \boldsymbol{y}_3,..., \boldsymbol{y}_m\}$ (m vertices in total), satisfying

$$k_1\boldsymbol{y}_1 + k_2\boldsymbol{y}_2 + \cdots + k_m\boldsymbol{y}_m = \boldsymbol{x}_i, \tag{2}$$

with $\sum_i k_i = 1$, $k_i \geqslant 0$. Note that the ACM correlation function $\overline{\Pi} = (\Pi_1, \Pi_2, \ldots, \Pi_n)$ satisfies $\sum_i \Pi_i = 1$ and $\Pi_i \geqslant 0$, indicating that all data points will be constrained in a finite $(n-1)$-dimensional hyperplane.

To ensure that all possible ground-state structures are included, we can enumerate supercells of various sizes and shapes until the convex hull no longer changes. As shown in the left of Fig. 2(b), there are only three structures by screening the candidates within eight atoms with the convex hull in the CE, and the corresponding coordinates are $(0, -1)$, $(-1, -1)$, and $(1, 1)$. However, we cannot be sure that whether the convex hull will change in larger cells. By contrast, we find three convex hull structures in the ACM, i.e., $(1, 0, 0)$, $(0, 1, 0)$, and $(0, 0, 1)$, respectively, as shown in the right of Fig. 2(b). They are located on the axis of correlation function space. It can be concluded that the current convex hull is complete, and the convex hull will remain the same even searching larger cells. Note that these structures on the axis are composed of only one type of cluster, exhibiting high symmetry in geometry.

In the framework of the ACM, there is a key index l, i.e., the number of nonzero components of correlation functions. The convex hull is complete if the number of structures with $l = 1$ is equal to the dimensionality of space because all the possible candidates can be linearly represented by these structures. Besides the 1D atom chain (shown in Fig. 2), there are three additional cases: two-dimensional (2D) square lattice, 2D triangular lattice, and three-dimensional fcc lattice with the certain R_{cut} (see SM, Secs. 4.1–4.3) [29].

When the number of structures with $l = 1$ is less than the dimensionality of space, we can classify the structures according to the dimensionality of l because all the data points in the ACM correlation function space are restricted to a finite hyperplane, and those with larger l are distributed inside the hyperplane. Note that $\overline{\Pi}_{\text{ACM}}$ with smaller l cannot be linearly represented by the ones with larger l and the convex hull can be solved in the order of l increasing sequences, making the search memorable. Furthermore, we can decompose the high-dimensional correlation function space into a combination of subspaces according to nonzero components of the correlation functions and determine the vertices in each subspace gradually.

Based on the above ideas, we have designed an algorithm from generating structures to calculating convex hull with the flow chart shown in Fig. 3. We propose a "jigsaw puzzle" to directly generate structures with small l to improve the search efficiency. Beginning from one position in a given cell, the clusters gradually are added outwards, and the selection of the cluster environment is arbitrary permutation and the combination under the restriction of the ACM generating group. Finally, the puzzle is completed, and the duplicate structures are filtered out based on symmetry, clearly minimizing the cost of producing candidates. The details about the algorithm are described in SM, Sec. 3 [29].

Taking the two-dimensional triangular lattice as an example, we study the evolution of ordered structures in the binary alloy system (A_xB_{1-x}) as the R_{cut} increases (see SM, Sec. 4.2 [29]). When the truncated environment of three atoms [see Fig. S14(a)] of the SM [29] is selected, there are four types of unique atomic clusters and four vertex structures corresponding to $l = 1$, indicating a complete convex hull

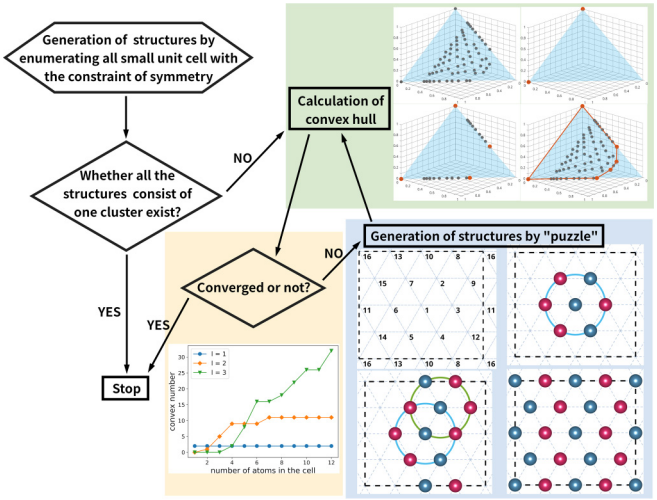

FIG. 3. The flow chart of determining the convex based on the ACM.

in this case. Selecting a truncated environment with seven atoms, the number of unique atomic clusters increases to 26, and only the pure phases containing only A or B atoms correspond to $l = 1$. According to the above algorithm, we have determined all possible vertex structures with $l = 2$. As shown in Fig. S14(b) of the SM [29], the structures b_6, b_7, and b_3 correspond to the ordered structures $(\sqrt{3} \times \sqrt{3})$, (2×2), and $(\sqrt{7} \times \sqrt{7})$ that alkali-metal atoms adsorbed on graphite in the experiments [31]. As shown in Figs. S14(c) and S14(d) of the SM [29], structure b_3 is not a vertex structure when the truncated environment is three atoms because it can be linearly expressed by the structures of a_2 and a_4 with $l = 1$. With the truncation environment of seven atoms, a_4 is convex with $l = 1$, whereas the l of vertex structure a_2 increases from 1 to 2. As a result, the structure b_3 becomes an additional vertex structures with $l = 2$ in the new correlation function space.

It can be comprehensible that the degenerate structures in the correlation function space with smaller R_{cut} will be distinguished by the increasing of R_{cut}, and new ground states will be uncovered. The number of nonzeros component l of the structure may increase with the R_{cut}, but the upper limit of l is the number of Wyckoff sites of the structure, corresponding to the infinite R_{cut}. According to the convex hull of the ACM, the candidates with small l will be ground states with more probability where smaller l corresponds to higher symmetry of the crystal structure. This explains very well why stable structures are usually considered to be highly symmetrical simply geometrical, containing few atoms [17]. Counterintuitively, structures with small N_{W} do not only exist in unit cells with few atoms. For example, there is a unit cell of 16 atoms in a fcc lattice with only $N_{\text{W}} = 2$ (structures that cannot be reduced to a smaller unit cell). However, it is still difficult to generate all the possible candidates with small N_{W} with the increasing of cell size.

Based on the ACM with the convex hull analysis, we have demonstrated that the structures with smaller l will become ground-state structures with higher probability. As the R_{cut} increases, the index l will be converted to the number of Wyckoff positions, and, thus, the possible ground states can be

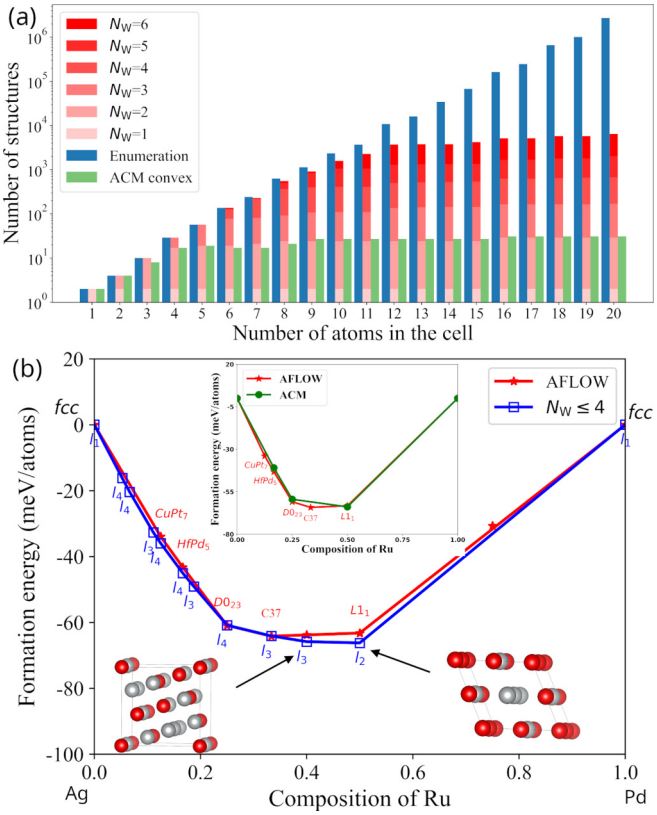

FIG. 4. (a) The comparison of the number of fcc-derivative structures between enumeration, the six-atom truncation ACM and the N_{W} classifications methods. (b) The convex hulls of formation energies for the Ag-Pd system. l_2, l_3, and l_4 indicate the structures with $N_{\text{W}} = 2$–4, respectively.

screened according to N_{W}. In our previous studies, the unique configurations are obtained by structural recognition [32]. To give a further screening of candidates, we provide two ways to calculate the ground-state structures of the alloy: (i) choose the ACM model with various R_{cut}'s and generate the vertex structures for the first-principles calculations; (ii) classify the structures by N_{W}, and gradually perform the calculations follow the order of N_{W} increasing sequences. Figure 4(a) shows the efficiency of the two strategies where the fcc-derivative structures are reduced from 10^6 to 10^2 and 10^3 for the unit cells within 20 atoms.

In the following, we will combine these two strategies with the first-principles calculations on alloys of Ag-Pd, Os-Ru, Ir-Ru, and Mo-Ru and compare with previous high-throughput calculations [33]. The candidates generation details are shown in SM Sec. 7 [29]. Figure 4(b) shows the formation energies of Ag-Pd (the results of Os-Ru, Ir-Ru, and Mo-Ru systems are shown in Fig. S17) of the SM [29] with the candidates from our two strategies, and the comparison with the previous calculations is demonstrated. In the first strategy, that is, screening structures by the ACM with a moderate R_{cut}, we only need to calculate a small amount of the structures and we can revisit the main results of AFLOW. For example, we only calculated 31 fcc-derivative structures for Ag-Pd [see the inset of Fig. 4(b)], 125 hcp-derivative structures for Os-Ru,

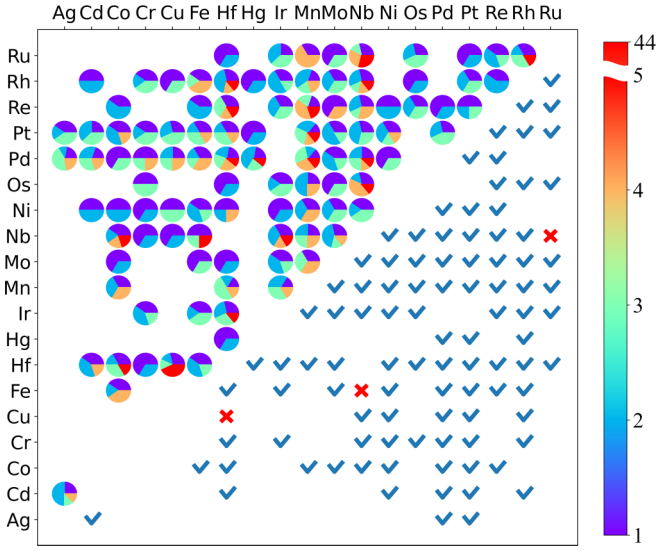

FIG. 5. The convex hull structures of formation energy from 100 binary systems are reclassified by N_W with their values shown in the color bars. The area of sector corresponds to the proportion of classified structures' number to that of all the ground states. The blue ticks are corresponding to the alloys satisfying the threshold whereas the red crosses do not.

156 structures (31 fcc and 125 hcp derivative) for Ir-Ru (see Fig. S17 in the SM Sec. 7 [29]).

According to the second strategy, the structures with $N_W \leqslant 4$ are calculated. Despite the higher computational cost with more structures, we reveal several as-yet unreported ordered states of Ag-Pd, Os-Ru, Ir-Ru, and Mo-Ru, whose formation energies are lower than those from AFLOW's results. Based on the calculations of 673 superstructures with the fcc derivative, there is a $Ag_{0.5}Pd_{0.5}$ structure with Fd-$3m$ symmetry which is more stable than $L1_1$, containing a unit cell of eight atoms with $N_W = 2$. Another stable $Ag_{0.6}Pd_{0.4}$ structure ($P4_2/n$) is found with a unit cell of 20 atoms and $N_W = 3$. [See Fig. 4(b).] Among the calculated 436 hcp-derivative structures of $Os_{1-x}Ru_x$, a new structure of $Os_{0.5}Ru_{0.5}$ ($Pnma$) was found to be more stable than B_{19}, and there are 16 atoms in its unit cell with $N_W = 4$. The structure of $Os_{1/3}Ru_{2/3}$($Cmcm$) is also stable according to the convex hull of formation energy, corresponding to a unit cell of six atoms and $N_W = 2$ [see Fig. S17(a)] of the SM [29].

For $Ir_{1-x}Ru_x$, we have performed the calculations of 673 fcc-derivative structures and 436 hcp-derivative structures. A new phase of $Ir_{1/3}Ru_{2/3}$ ($P6_3/mmc$) is found to be more stable than the phase of Ir_2Tc, possessing a unit cell of 18 atoms with $N_W = 3$ [see Fig. S17(b)] of the SM [29]. Based on the calculation of 682 bcc-derivative structures and 436 hcp-derivative structures, the most stable $Mo_{0.25}Ru_{0.75}$ corresponds to the bcc lattice, whose energy is very close to the hcp derivative from AFLOW's results. This new $Mo_{0.25}Ru_{0.75}$ structure possesses the symmetry of $Cmcm$ with eight atoms in the unit cell and $N_W = 3$. In addition, $Mo_{0.125}Ru_{0.875}$ (P-$6m2$) is found to be stable with a unit cell of eight atoms and and $N_W = 4$. [see Fig. S17(c)] of the SM [29].

To verify the generality of our method, we extract the ground-state structures with 100 binary systems (the combination of Ag, Cd, Co, Cr, Cu, Fe, Hf, Hg, Ir, Mn, Mo, Nb, Ni, Os, Pd, Pt, Re, and Rh) in AFLOW. For 82% of the systems, there are no ground-state structures with $N_W \geqslant 5$ (see Fig. 5). We define the success rate,

$$P = \frac{N_{gs}(N_W \leqslant 4)}{N_{gs}}, \tag{3}$$

where N_{gs} is the number of ground-state structures. With the threshold of 80%, only three binary alloys fail. For comparison, we consider the number of atoms in the cell and the number of symmetry operations (see Fig. S18 of the SM [29]). With the similar computational cost, about 30% of the alloy will fail when we consider the candidates with few atoms. The convex hull structures are not strongly associated with the number of symmetry operations. Thus, N_W is superior to these two indices.

To summarize, we demonstrate that ground states of the alloy can be feasibly determined based on the ACM, revealing the connection between stable alloys and geometric symmetry, i.e., the structures with lower l or N_W will become ground states with greater probability. The number of candidates for the first-principles calculations is remarkably reduced. According to the formation energies of Ag-Pd, Os-Ru, Ir-Ru, and Mo-Ru systems, we have predicted many configurations with higher stability. Our finding provides a standard routine to screen stable alloy structures, facilitating high-throughput first-principles calculations of alloys.

This work was supported by the National Key R&D Program of China (No. 2018YFB1502101), Guangdong Basic and Applied Basic Research Foundation (Grant No. 2021A1515010328), and the National Natural Science Foundation of China (Grant No. 12074126).

[1] C. J. Pickardand R. J. Needs, Ab initio random structure searching, J. Phys.: Condens. Matter **23**, 053201 (2011).

[2] A. R. Oganov and C. W. Glass, Crystal structure prediction using ab initio evolutionary techniques: Principles and applications, J. Chem. Phys. **124**, 244704 (2006).

[3] Y. Wang, J. Lv, L. Zhu, and Y. Ma, Crystal structure prediction via particle-swarm optimization, Phys. Rev. B **82**, 094116 (2010).

[4] L. Sun, M. R. G. Marques, M. A. L. Marques, and S. Botti, Point defects in hexagonal silicon, Phys. Rev. Mater. **5**, 064605 (2021).

[5] J. Sun, Z. Liao, Y. Zhang, Y. Guo, and X. Ke, First-principles study of pressure-induced phase transitions, mechanical and thermodynamic properties of ThBC, J. Phys.: Condens. Matter **34**, 044001 (2022).

[6] Y.-Q. Zhao, Y. Cheng, C.-E. Hu, B.-R. Yu, and G.-F. Ji, Structural exploration and properties of (bn)6 cluster via ab initio in combination with particle swarm optimization method, Theor. Chem. Acc. **140**, 51(2021).

[7] P. Gao, B. Gao, S. Lu, H. Liu, J. Lv, Y. Wang, and Y. Ma, Structure search of two-dimensional systems using CALYPSO methodology, Front. Phys. **17**, 23203 (2022).

[8] A. van de Walle, Multicomponent multisublattice alloys, nonconfigurational entropy and other additions to the alloy theoretic automated toolkit, Calphad **33**, 266 (2009).
[9] G. Hart, V. Blum, M. Walorski, and A. Zunger, Evolutionary approach for determining first-principles hamiltonians, Nature Mater. **4**, 391 (2005).
[10] T. Mueller and G. Ceder, Bayesian approach to cluster expansions, Phys. Rev. B **80**, 024103 (2009).
[11] X. Yangand J. Ni, Ground states of adsorbates on single-walled carbon nanotubes, Phys. Rev. B **67**, 195403 (2003).
[12] M. Kaburagi and J. Kanamori, A method of determining the ground state of the extended-range classical lattice gas model, Prog. Theor. Phys. **54**, 30 (1975).
[13] J. Kanamori, Infinite series of ground states of the ising model on the honeycomb lattice, J. Phys. Soc. Jpn. **53**, 250 (1984).
[14] U. Brandt and J. Stolze, Ground states of the Triangular Ising model with two-and three-spin interactions, Z. Phys. B: Condens. Matter **64**, 481 (1986).
[15] J. Stolze, Oxygen Ordering in the Basal Plane of $YBa_2Cu_3O_z$: Ground States, Phys. Rev. Lett. **64**, 970 (1990).
[16] A. Seko, K. Shitara, and I. Tanaka, Efficient determination of alloy ground-state structures, Phys. Rev. B **90**, 174104 (2014).
[17] G. L. W. Hart, Where are nature's missing structures? Nature Mater. **6**, 941 (2007).
[18] A. P. Bartók, M. C. Payne, R. Kondor, and G. Csányi, Gaussian Approximation Potentials: The Accuracy of Quantum Mechanics, without the Electrons, Phys. Rev. Lett. **104**, 136403 (2010).
[19] T. Xie and J. C. Grossman, Crystal Graph Convolutional Neural Networks for an Accurate and Interpretable Prediction of Material Properties, Phys. Rev. Lett. **120**, 145301 (2018).
[20] L. Zhang, J. Han, H. Wang, R. Car, and W. E, Deep Potential Molecular Dynamics: A Scalable Model with the Accuracy of Quantum Mechanics, Phys. Rev. Lett. **120**, 143001 (2018).
[21] J. Yoon and Z. W. Ulissi, Differentiable Optimization for the Prediction of Ground State Structures (DOGSS), Phys. Rev. Lett. **125**, 173001 (2020).
[22] N. A. Zarkevich and D. D. Johnson, Reliable First-Principles Alloy Thermodynamics via Truncated Cluster Expansions, Phys. Rev. Lett. **92**, 255702 (2004).
[23] H. Edelsbrunner and N. R. Shah, Incremental topological flipping works for regular triangulations, Algorithmica **15**, 223 (1996).
[24] C. B. Barber, D. P. Dobkin, and H. Huhdanpaa, The quickhull algorithm for convex hulls, ACM Trans. Math. Softw. **22**, 469 (1993).
[25] C.-C. He, J.-S. Y. Shao-Bin. Qiu, J.-H. Liao, Y.-J. Zhao, and X.-B. Yang, Atom classification model for total energy evaluation of two-dimensional multicomponent materials, J. Phys. Chem. A **124**, 4506 (2020).
[26] G. Kresse and J. Hafner, Ab initio molecular dynamics for open-shell transition metals, Phys. Rev. B **48**, 13115 (1993).
[27] G. Kresse and D. Joubert, From ultrasoft pseudopotentials to the projector augmented-wave method, Phys. Rev. B **59**, 1758 (1999).
[28] J. P. Perdew, K. Burke, and M. Ernzerhof, Generalized Gradient Approximation Made Simple, Phys. Rev. Lett. **77**, 3865 (1996).
[29] See Supplemental Material at http://link.aps.org/supplemental/10.1103/PhysRevMaterials.6.L050801 for details on the whole process from the construction of ACM to the first-principles calculations.
[30] J. Sivardière and J. Lajzerowicz, Spin-1 lattice-gas model. ii. condensation and phase separation in a binary fluid, Phys. Rev. A **11**, 2090 (1975).
[31] Z. P. Hu, N. J. Wu, and A. Ignatiev, Cesium adsorption on graphite (0001) surface: The phase diagram, Phys. Rev. B **33**, 7683 (1986).
[32] C.-C. He, J.-H. Liao, S.-B. Qiu, Y.-J. Zhao, and X.-B. Yang, Biased screening for multi-component materials with structures of alloy generation and recognition (SAGAR), Comput. Mater. Sci. **193**, 110386 (2021).
[33] G. L. W. Hart, S. Curtarolo, T. B. Massalski, and O. Levy, Comprehensive Search for New Phases and Compounds in Binary Alloy Systems Based on Platinum-Group Metals, Using a Computational First-Principles Approach, Phys. Rev. X **3**, 041035 (2013).